



Periodic and Chaotic Dynamics of the Ehrhard–Müller System

Junho Park*, Hyunho Lee and Jong-Jin Baik

School of Earth and Environmental Sciences,

Seoul National University,

Seoul 151-742, Republic of Korea

**junho.park@snu.ac.kr*

Received September 14, 2015; Revised December 7, 2015

This paper investigates nonlinear ordinary differential equations of the Ehrhard–Müller system which describes natural convection in a single-phase loop in the presence of nonsymmetric heating. Stability and dynamics of periodic and chaotic behaviors of the equations are investigated and the periodicity diagram is obtained in wide ranges of parameters. Regimes of both periodic and chaotic solutions are observed with complex behaviors such that the periodic regimes enclose the chaotic regime while they are also immersed inside the chaotic regime with various shapes. An asymptotic analysis is performed for sufficiently large parameters to understand the enclosure by the periodic regimes and asymptotic limit cycles are obtained to compare with limit cycles obtained from numerical results.

Keywords: Ehrhard–Müller system; stability analysis; chaotic dynamics; periodicity diagram; asymptotic analysis.

1. Introduction

Natural convection in a single-phase loop occurs when the bottom of the loop is heated while the top is cooled, and has been investigated in numerous works since it serves as a fundamental dynamical model for nuclear reactors, geothermal power system, solar heating system, etc. [Zvirin, 1982; Basu *et al.*, 2014]. Although the system is very simple, the fluid flow inside the loop exhibits chaotic behaviors so it has led to many theoretical investigations. After [Welander, 1967] who firstly studied oscillatory instability occurring in the differentially heated loop, there have been many experiments on this system which have revealed its chaotic behavior [Gorman *et al.*, 1984, 1986; Widmann *et al.*, 1989] which is typically observed in other phenomena in hydrodynamics such as the circular Couette flow [Gollub & Swinney, 1975], the Rayleigh–Bénard

convection [Lorenz, 1963], etc. Moreover, [Malkus, 1972] and [Yorke & Yorke, 1981] derived a simple set of nonlinear ordinary differential equations, the equations analogous to the Lorenz equations with the geometric parameter $b = 1$ [Lorenz, 1963; Yorke *et al.*, 1987], to understand the physics of the chaotic convection inside the loop. The equations were extended to more general cases with nonsymmetric heating by [Ehrhard & Müller, 1990], known as the Ehrhard–Müller system which suggests the following nonlinear differential equations:

$$\dot{x} = \sigma(y - x), \quad (1)$$

$$\dot{y} = rx - xz - y + c, \quad (2)$$

$$\dot{z} = xy - z, \quad (3)$$

where x , y and z are the dynamic variables, dot denotes the derivative with respect to time t , σ is

*Author for correspondence

the parameter which relates the wall friction coefficient to the heat transfer coefficient, r is the heating rate and $c = r \tan \delta$ is the heating ratio with tilting angle δ of the loop. When the heating is symmetric (i.e. the bottom is heated while the top is cooled), the angle δ is zero (i.e. $c = 0$) while δ is nonzero when the heating is nonsymmetric due to the tilted loop. Ehrhard and Müller [1990] studied bifurcation behaviors of (1)–(3) which show good agreements with experiments for both symmetric and nonsymmetric heating. They found that onset of flow instability in the loop is delayed as the heating becomes nonsymmetric. The natural convection with the nonsymmetric heating has also been studied in a tilted square loop in which chaotic flow patterns are also observed [Acosta *et al.*, 1987].

Although (1)–(3) are too simplified to exhibit the real physics of the natural convection in the heated single-phase loop, it is still worth to investigate periodic and chaotic behaviors of such equations, for instance, to study distinct scenarios of transition to turbulence as investigated in the nonsymmetric Lorenz model [Shil'nikov & Shil'nikov, 1991]. Equations (1)–(3) can also be regarded as the controlled Lorenz equations with constant forcing c [Zhu & Tian, 2005]. Thus, it is worth to investigate the effects of the parameter c for the purpose of chaos control. Since only brief studies on the stability and the bifurcation characteristics were performed [Ehrhard & Müller, 1990; Shil'nikov & Shil'nikov, 1991], we investigate periodic and chaotic dynamics of (1)–(3) in wide ranges of parameters r and c . In this paper, the parameter σ is fixed as $\sigma = 15$, same as [Ehrhard & Müller, 1990], and parametric study with σ is not performed as it was done in other work for $c = 0$ [Dullin *et al.*, 2007]. In Sec. 2, we analyze the stability of the system and in Sec. 3, we define periodicity of the solutions following [Zhou *et al.*, 1997a; Park *et al.*, 2015] and obtain the periodicity diagram from numerical integrations. Asymptotic analysis is performed in Sec. 4 to understand the dynamics of the equations for large values of parameters r and c .

2. Stability Analysis and Trajectories

Firstly, we analyze the stability of (1)–(3). Due to the symmetry $(x, y, z, c) = (-x, -y, z, -c)$, we hereafter consider only non-negative c . Applying $\dot{x} = \dot{y} = \dot{z} = 0$, we obtain three equilibrium points

(x_0, y_0, z_0) which satisfy the following:

$$x_0^3 - (r - 1)x_0 - c = 0, \quad y_0 = x_0, \quad z_0 = x_0^2. \quad (4)$$

The cubic equation of x_0 in (4) has a solution of the form $x_0 = w + (r - 1)/(3w)$ where w satisfies

$$w^3 = \frac{c}{2} \pm \sqrt{\frac{c^2}{4} - \frac{(r - 1)^3}{27}}. \quad (5)$$

This implies that there is only one equilibrium point on the real plane if $c^2 > 4(r - 1)^3/27$, or there are three equilibrium points otherwise. We define the equilibrium points x_1 , x_2 and x_3 in descending order of real part of x_0 .

Figures 1(a)–1(d) show illustrations of the curve $f(x_0) = x_0^3 - (r - 1)x_0 - c$ for different parameters r and c to see locations of the three equilibrium points x_1 , x_2 and x_3 . We see that there exists only one point x_1 if $c^2 > 4(r - 1)^3/27$. Moreover, the points x_1 and x_3 are symmetric with respect to $x_2 = 0$ at $c = 0$ while the symmetry breaks for $c > 0$.

Applying infinitesimal perturbations x' , y' and z' to the equilibrium points as $x = x_0 + x'$, $y = y_0 + y'$ and $z = z_0 + z'$, we obtain the following linearized equations:

$$\frac{d}{dt} \begin{bmatrix} x' \\ y' \\ z' \end{bmatrix} = \begin{bmatrix} -\sigma & \sigma & 0 \\ r - z_0 & -1 & -x_0 \\ y_0 & x_0 & -1 \end{bmatrix} \begin{bmatrix} x' \\ y' \\ z' \end{bmatrix}. \quad (6)$$

From the modal expression $(x', y', z') = (\tilde{x}, \tilde{y}, \tilde{z}) \times \exp(\lambda t) + \text{c.c.}$, where λ is the growth rate and c.c. denotes the complex conjugate, we obtain the growth rate λ and the corresponding neutral stability curves where the real part of λ becomes zero for three equilibrium points. For $c > 0$, the neutral stability curves have analytical expressions in very complex forms so we compute these curves numerically.

Figure 1(e) shows stability regimes divided by the neutral stability curves in the parameter space (r, c) for $\sigma = 15$. In regime I, there is only one equilibrium point x_1 which is stable and two equilibrium points x_2 and x_3 are not located on the real plane. Regime II has one stable point x_1 and two unstable points x_2 and x_3 while regime III has two stable points x_1 , x_3 and one unstable point x_2 . In fact, the curve dividing regime I and regimes II and III is $c^2 = 4(r - 1)^3/27$, which implies that the point x_2 becomes always unstable as it appears on the real

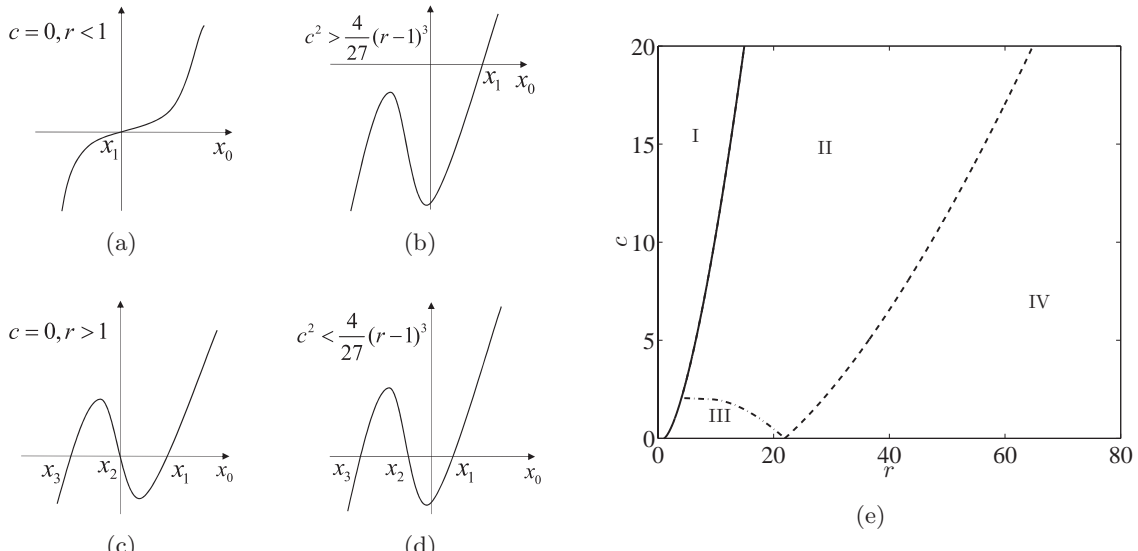


Fig. 1. (a)–(d) Illustrations of the curve $f(x_0) = x_0^3 - (r - 1)x_0 - c$ and the equilibrium points x_1, x_2 and x_3 for different parameters r and c : (a) $c = 0, r < 1$, (b) $c^2 > \frac{4}{27}(r-1)^3/27$, (c) $c = 0, r > 1$ and (d) $c^2 < \frac{4}{27}(r-1)^3/27$. (e) Regimes of stability in the parameter space (r, c) for $\sigma = 15$ with neutral stability curves: dashed, solid and dash-dot lines represent the neutral stability curves where the equilibrium points x_1, x_2 and x_3 become unstable, respectively.

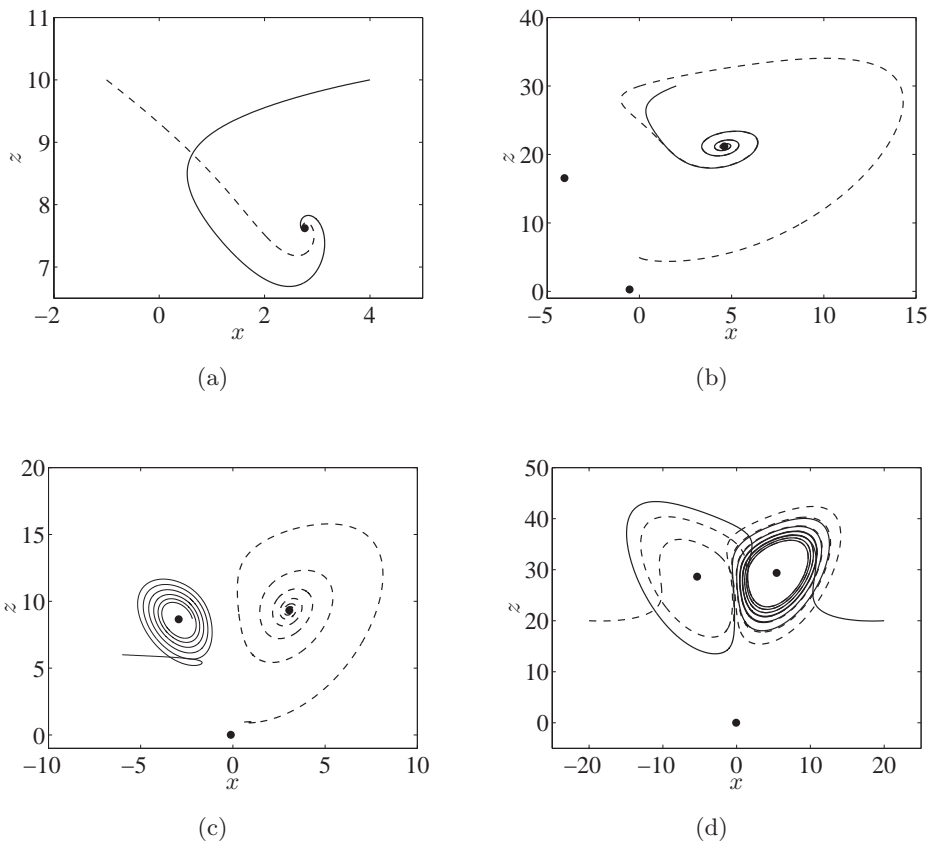


Fig. 2. Examples of trajectories on the x - z plane in (a) regime I ($r = 5, c = 10$), (b) regime II ($r = 20, c = 10$), (c) regime III ($r = 10, c = 1$) and (d) regime IV ($r = 30, c = 2$). Time integrations are performed from $t = 0$ to $t = 10$ with initial conditions $y = 0$ and (a) $(x, z) = (4, 10)$ (solid), $(x, z) = (-1, 10)$ (dashed), (b) $(x, z) = (2, 30)$ (solid), $(x, z) = (0, 4)$ (dashed), (c) $(x, z) = (-6, 6)$ (solid), $(x, z) = (1, 1)$ (dashed) and (d) $(x, z) = (20, 20)$ (solid), $(x, z) = (-20, 20)$ (dashed). Dots represent equilibrium points.

plane. On the other hand, the point x_3 is not always unstable but stable in regime III. In regime IV, all the equilibrium points are unstable.

To more clearly understand the dynamical behaviors for each regime, trajectories of the solutions on the x - z plane are obtained for different values of parameters r and c (Fig. 2). Two different initial conditions are tested at each regime with time integrations from $t = 0$ to $t = 10$ with numerical parameters detailed in the next section. Figure 2(a) shows that all the trajectories converge to the equilibrium point x_1 in regime I. This behavior is the same in regime II except that the other two unstable equilibrium points x_2 and x_3 now exist on the real plane [Fig. 2(b)]. In regime III, trajectories converge to either x_1 or x_3 depending on initial conditions [Fig. 2(c)]. Figure 2(d) shows that all equilibrium points are unstable in regime IV so that trajectories do not converge to the equilibrium points but they orbit around points x_1 and x_3 with periodic or chaotic behaviors which represent periodic limit cycles or chaotic attractors, respectively. In the following section, we analyze more details on the solutions in regime IV to investigate periodic and chaotic dynamics of (1)–(3).

3. Numerical Analysis

Numerical integrations of (1)–(3) are performed with MATLAB using the fourth order Runge–Kutta method with a time resolution $\Delta t = 5 \cdot 10^{-4}$ and initial conditions $(x_0, y_0, z_0) = (10^{-2}, 0, r - 1)$. These numerical parameters are sufficient to capture periodic and chaotic dynamics of (1)–(3) in the parameter space of our interest. To ignore nonsteady behaviors in initial stage, the initial data from $t = 0$ to $t = 200$ are truncated and the data from $t = 200$ to $t = 250$ are used. In such a way, the solutions lie on either limit cycles or chaotic attractors [Yu *et al.*, 1996; Zhou *et al.*, 1997b]. We also tested other initial conditions and verified that all the solutions lie on the periodic limit cycles or on the chaotic attractors after $t = 200$ in the parameter space of our interest. Following [Yu *et al.*, 1996; Zhou *et al.*, 1997b; Park *et al.*, 2015], we define periodicity of the solutions as the number of z_{\max} , the maximum values of z . From the data from $t = 200$ to $t = 250$, local maximum values z_{\max} are picked for each integration. The period is distinguished if the values of z_{\max} differ with a relative tolerance more than 0.1%.

Figures 3(a)–3(e) show examples of limit cycles with different periods and chaotic attractors for different values of c at $r = 2000$. At $c = 0$, the limit cycle in Fig. 3(a) is symmetric with respect to $x = 0$ and has period 1 since it has only one z_{\max} about 2116.8. On the other hand, the limit cycle in Fig. 3(b) at $c = 200$ has period 2 with one maximum about 2095.0 and the other about 2144.6 and it is no longer symmetric with respect to $x = 0$ for $c > 0$. As c increases, the period increases to 4 [Fig. 3(c)] and the solutions become chaotic [Fig. 3(d)]. For the chaotic attractors, the period cannot be defined since the number of z_{\max} increases as more time integrations are performed. Then, the solutions become periodic (or stable) as c increases further. Note that there are not only limit cycles with periods of power of two but also with periods of 3, 5, 6 [e.g. Fig. 3(e)] or higher numbers. To see how the period changes as c increases, the bifurcation diagram of z_{\max} at $r = 2000$ is obtained [Fig. 3(f)]. We clearly see that the forward bifurcation starts from $c = 0$ and this is due to the broken symmetry of the limit cycle for $c > 0$ as shown in Fig. 3(b). Then, the second forward bifurcation starts at $c = 394$ and the chaotic behavior appears around $c \sim 580$ and finishes around $c \sim 2580$. Interestingly, not only the periodic windows inside the chaotic regime appear, a typical characteristic of the nonlinear dynamical systems [Zhou *et al.*, 1997b], but also disconnected bifurcations appear both inside and outside the chaotic regime [Park *et al.*, 2015].

To understand the periodic and chaotic behaviors in wide ranges of parameters, periodicity diagrams are obtained in the r - c parameter space as shown in Fig. 4 [Dullin *et al.*, 2007; Park *et al.*, 2015]. Period of the solutions is distinguished from 1 to 8 by different colors and by yellow for periods from 9 to 16. There are solutions with periods higher than 16 but they cover very little areas in the diagram and become chaotic immediately; therefore, they are difficult to be distinguished from the chaotic solutions. Thus, they are colored by white same as chaotic solutions. Regimes I, II and III are colored by black and are separated by a blue dashed line same as the dashed line in Fig. 1(e).

Figure 4(a) shows a periodicity diagram with resolutions $\Delta r = \Delta c = 10$. Although such resolutions are not sufficient to observe very small structures such as narrow periodic windows [Yu *et al.*, 1996], we see at a glance rough structures

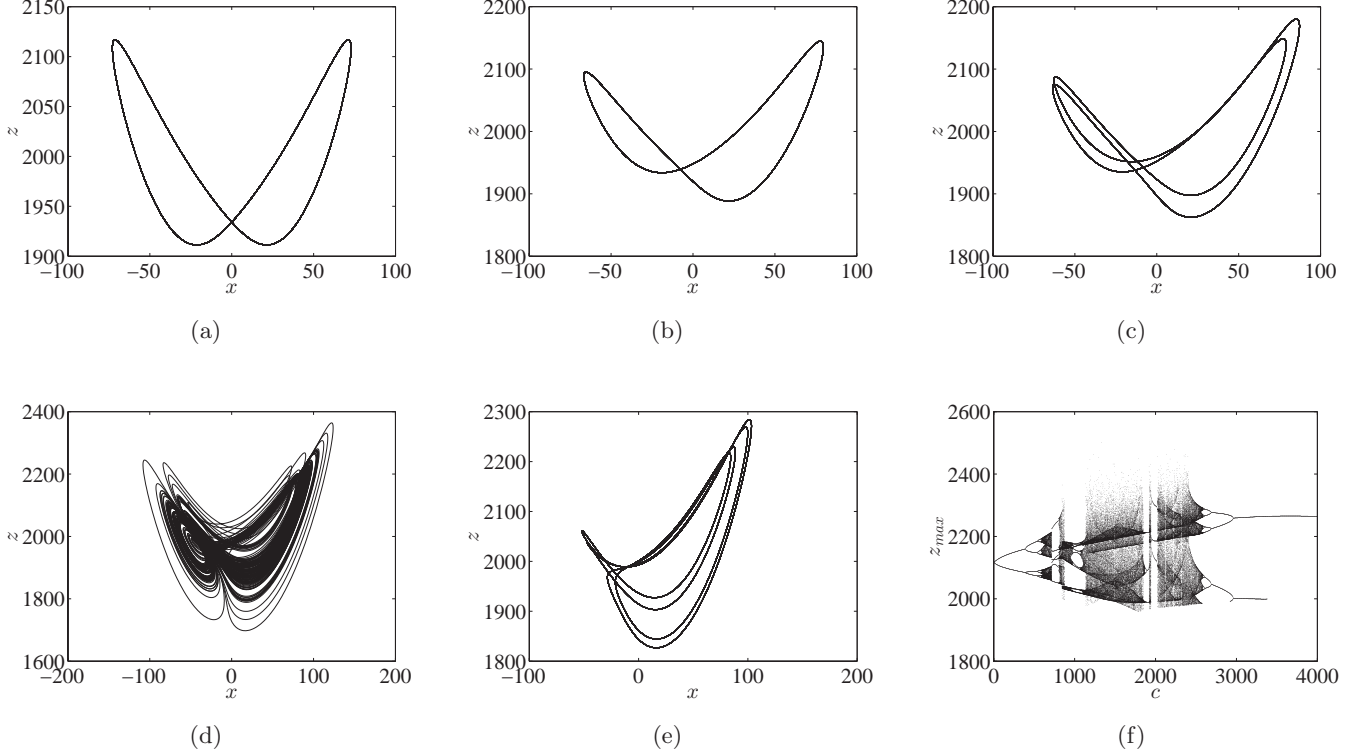


Fig. 3. (a)–(e) Examples of limit cycles and chaotic attractors on the x - z plane at $r = 2000$ and at (a) $c = 0$ (period 1), (b) $c = 200$ (period 2), (c) $c = 500$ (period 4), (d) $c = 1500$ (chaotic) and (e) $c = 2650$ (period 6). (f) Bifurcation diagram of z_{\max} at $r = 2000$ in the range $0 \leq c \leq 4000$.

of regimes of periodic and chaotic solutions in wide ranges of parameters. For a fixed c , solutions with period 1 firstly appear and they become periodic with higher periods or chaotic as r increases. But

then, solutions become periodic again with period 2 (period 1, if $c = 0$) for sufficiently large r . It is clearly seen that the chaotic regime is enclosed by the regimes of periodic solutions so that solutions

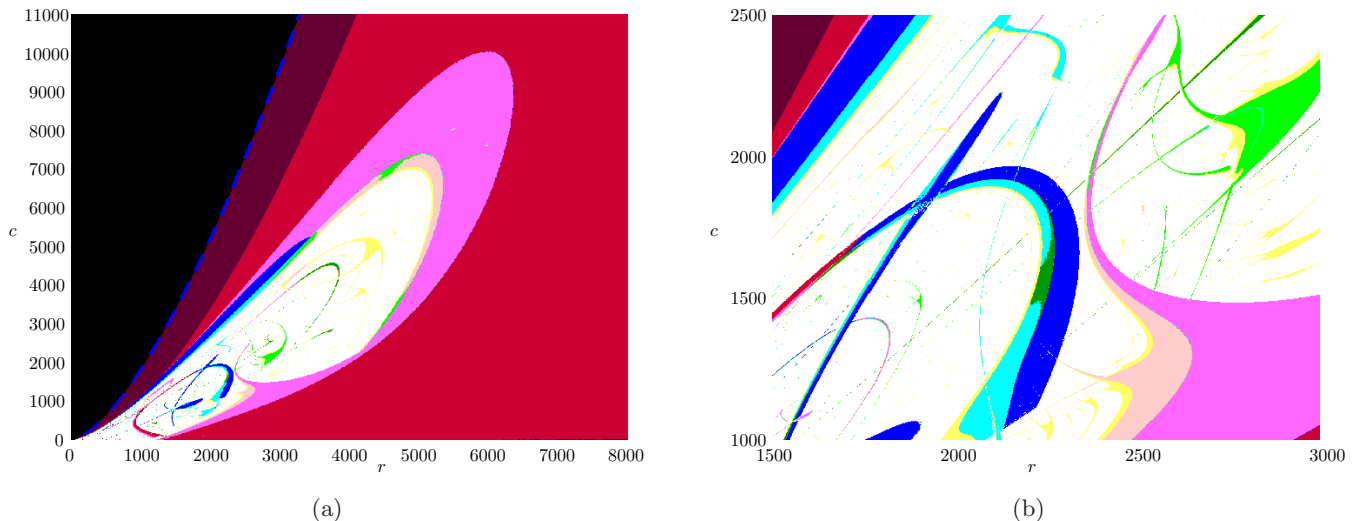


Fig. 4. Periodicity diagrams in the r - c parameter space for (a) $0 \leq r \leq 8000$ and $0 \leq c \leq 11000$ with resolutions $\Delta r = \Delta c = 10$ and for (b) $1500 \leq r \leq 3000$ and $1000 \leq c \leq 2500$ with resolutions $\Delta r = \Delta c = 1$. Colors indicate the periodicity of solutions: fixed solutions (black), period 1 (dark red), period 2 (red), period 3 (blue), period 4 (pink), period 5 (dark green), period 6 (cyan), period 7 (light green), period 8 (light pink), period 9 to 16 (yellow), period higher than 16 or chaotic solutions (white). Blue dashed line represents a neutral stability curve same as the dashed line in Fig. 1.

become periodic for large parameters $r > 5340$ or $c > 7390$ as shown in Fig. 4(a). Figure 4(b) displays a zoomed view of the chaotic regime with finer resolutions $\Delta r = \Delta c = 1$. Interestingly, inside the chaotic regime, there exist immersed periodic regimes with shapes of curved bands [Park *et al.*, 2015], shrimp-shape islands [Xavier & Rech, 2010], narrow periodic windows [Zhou *et al.*, 1997b], etc. These complex structures appear irregularly and unpredictably and are one of the typical characteristics observable in other chaotic systems such as the Lorenz–Stenflo system [Xavier & Rech, 2010; Park *et al.*, 2015], the Hénon map [Gallas, 1993], the CO₂ laser system [Bonatto *et al.*, 2005] or the Chua’s circuit [Albuquerque *et al.*, 2008].

To further investigate chaotic dynamics of (1)–(3), the Lyapunov exponents are computed using the continuous Gram–Schmidt orthonormalization (CGSO) method [Christiansen & Rugh, 1997]. We validated the code in this paper with other code for the Lorenz equations [Meador, 2011]. To obtain the Lyapunov exponents, 1000 random initial conditions are used with time integrations from $t = 0$

to $t = 1200$ with a resolution $\Delta t = 10^{-3}$. The initial data are also truncated and only the data from $t = 200$ to $t = 1200$ are used to compute all the three Lyapunov exponents. This time range from $t = 200$ to $t = 1200$ is large enough to compute the Lyapunov exponents [Meador, 2011]. Figure 5(a) shows bifurcation diagram of z_{\max} at $c = 1700$ in the range $1500 \leq r \leq 3000$ with resolution $\Delta r = 1$. With this resolution, both chaotic solutions and narrow periodic windows are well captured in this range of r . Figures 5(b)–5(d) show the Lyapunov exponents λ_1 , λ_2 and λ_3 where $\lambda_1 > \lambda_2 > \lambda_3$. We clearly see that for chaotic solutions, the maximum Lyapunov exponent λ_1 is positive while it is zero for periodic solutions. On the other hand, the second exponent λ_2 is zero for chaotic solutions while it becomes negative for periodic solutions. In theory, these exponents should satisfy $\lambda_1 + \lambda_2 + \lambda_3 = -\sigma - 1 - 1$, the sum of diagonal terms of the matrix in (6) [Lorenz, 1963], so that the minimum Lyapunov exponent λ_3 is always negative and changes in accord with λ_1 and λ_2 satisfying this relation. For each computation, the code checks that the sum

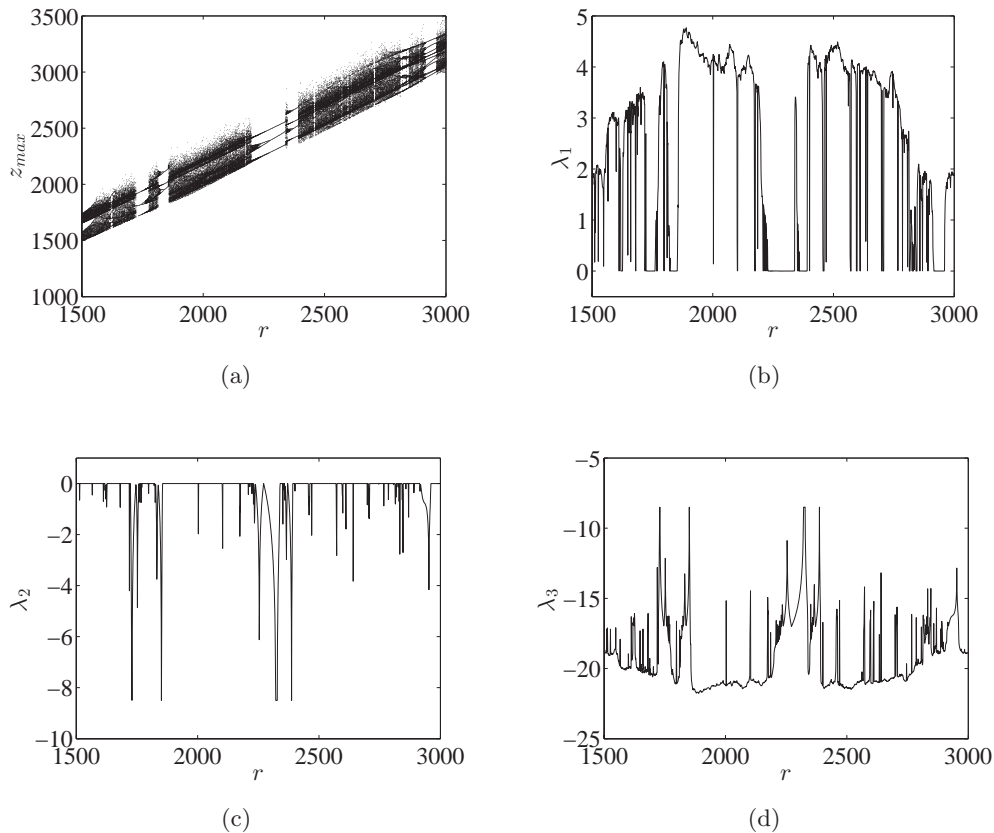


Fig. 5. (a) Bifurcation diagram of z_{\max} in the range $1500 \leq r \leq 3000$ at $c = 1700$. Only the time integration from $t = 200$ to $t = 210$ is performed to plot the diagram. (b)–(d) The Lyapunov exponents (b) λ_1 , (c) λ_2 and (d) λ_3 in the range $1500 \leq r \leq 3000$ at $c = 1700$.

$\lambda_1 + \lambda_2 + \lambda_3$ is equal to $-\sigma - 2$ with error of order $O(10^{-5})$.

4. Asymptotic Analysis for Limit Cycles

In this section, we perform an asymptotic analysis to understand why the solutions become periodic for sufficiently large parameters following [Shimizu, 1979] who asymptotically investigated limit cycles of the Lorenz system. New variables are introduced for large r as

$$\begin{aligned} X &= \frac{x}{\sqrt{2\sigma(r-1)}}, & Y &= \frac{z}{(r-1)-X^2}, \\ Z &= \frac{dx}{d\tau}, \end{aligned} \quad (7)$$

where $\tau = t/\epsilon$ and $\epsilon = 1/\sqrt{\sigma(r-1)}$. Then, (1)–(3) can be rescaled as

$$\frac{dX}{d\tau} = Z, \quad (8)$$

$$\frac{dY}{d\tau} = -\epsilon(Y - X^2), \quad (9)$$

$$\frac{dZ}{d\tau} = -X(X^2 + Y - 1) + C - \epsilon(\sigma + 1)Z, \quad (10)$$

where $C = c/\sqrt{2\sigma(r-1)^3}$. By expanding the variables

$$X = X_0 + \epsilon X_1 + \dots, \quad (11)$$

$$Y = Y_0 + \epsilon Y_1 + \dots, \quad (12)$$

$$Z = Z_0 + \epsilon Z_1 + \dots, \quad (13)$$

we obtain the equations at leading order

$$\frac{dX_0}{d\tau} = Z_0, \quad (14)$$

$$\frac{dY_0}{d\tau} = 0, \quad (15)$$

$$\frac{dZ_0}{d\tau} = -X_0(X_0^2 + Y_0 - 1) + C \quad (16)$$

and at the next order

$$\frac{dX_1}{d\tau} = Z_1, \quad (17)$$

$$\frac{dY_1}{d\tau} = -Y_0 + X_0^2, \quad (18)$$

$$\begin{aligned} \frac{dZ_1}{d\tau} &= -(\sigma + 1)Z_0 \\ &\quad - (3X_0^2 + Y_0 - 1)X_1 - X_0Y_1. \end{aligned} \quad (19)$$

Note that Y_0 is now a constant to be determined. Assume that the system lies on a limit cycle $\phi(X, Y, Z, \epsilon) = K(\epsilon)$ where both ϕ and K can be expanded as

$$\begin{aligned} \phi(X, Y, Z, \epsilon) &= \phi_0(X, Y, Z) \\ &\quad + \epsilon\phi_1(X, Y, Z) + \dots, \end{aligned} \quad (20)$$

$$K(\epsilon) = K_0 + \epsilon K_1 + \dots \quad (21)$$

From (14)–(16), the following relation is satisfied as

$$\begin{aligned} X_0^3 \frac{dX_0}{d\tau} + Y_0 X_0 \frac{dX_0}{d\tau} - X_0 \frac{dX_0}{d\tau} \\ - C \frac{dX_0}{d\tau} + Z_0 \frac{dZ_0}{d\tau} = 0, \end{aligned} \quad (22)$$

which leads to an expression of the limit cycle at leading order as

$$\begin{aligned} \phi_0(X_0, Y_0, Z_0) &= X_0^4 + 2(Y_0 - 1)X_0^2 \\ &\quad - 4CX_0 + 2Z_0^2 = K_0. \end{aligned} \quad (23)$$

The expression (23) implies that (1)–(3) have solutions which lie on the limit cycle (23) when r is sufficiently large for a fixed C (i.e. when c is large with order $O((r-1)^{3/2})$). To find the limit cycle, the constants K_0 and Y_0 should be determined. We consider ϕ_1 which can be found by matching (20) and (21):

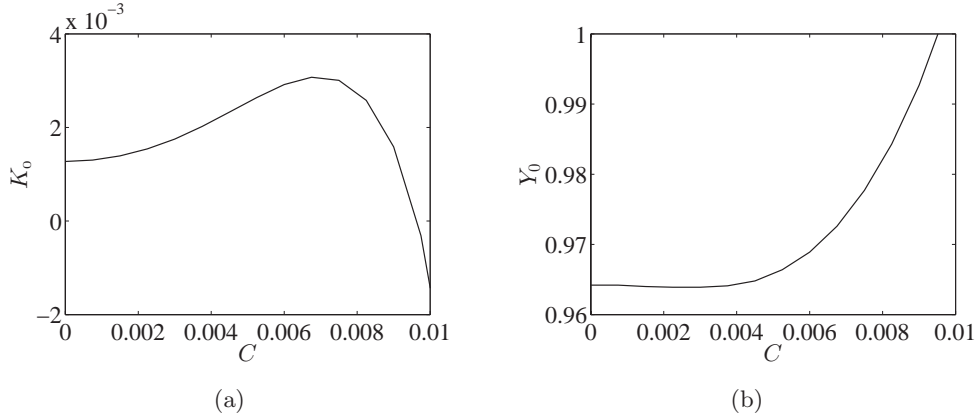
$$\phi_1(X_0, Y_0, Z_0) + \frac{\partial\phi_0}{\partial X_0}X_1 + \frac{\partial\phi_0}{\partial Y_0}Y_1 + \frac{\partial\phi_0}{\partial Z_0}Z_1 = K_1. \quad (24)$$

Differentiating (24) with respect to the rescaled time τ , ϕ_1 satisfies

$$\frac{d\phi_1}{d\tau} = 2X_0^2(Y_0 - X_0^2) + 4(\sigma + 1)Z_0^2. \quad (25)$$

Note that $d\phi_1/d\tau$ is expressed only by the leading order terms X_0 , Y_0 and Z_0 . We then can compute the period of the limit cycle T using the relation

$$\begin{aligned} \dot{X}_0 &= Z_0 \\ &= \pm \sqrt{-\frac{1}{2}X_0^4 + (1 - Y_0)X_0^2 + 2CX_0 + \frac{1}{2}K_0}, \end{aligned} \quad (26)$$

Fig. 6. Constants (a) K_0 and (b) Y_0 as a function of C at $\sigma = 15$.

which leads to

$$T = 2 \int_{x_1}^{x_2} \frac{dX_0}{\sqrt{-\frac{1}{2}X_0^4 + (1 - Y_0)X_0^2 + 2CX_0 + \frac{1}{2}K_0}}, \quad (27)$$

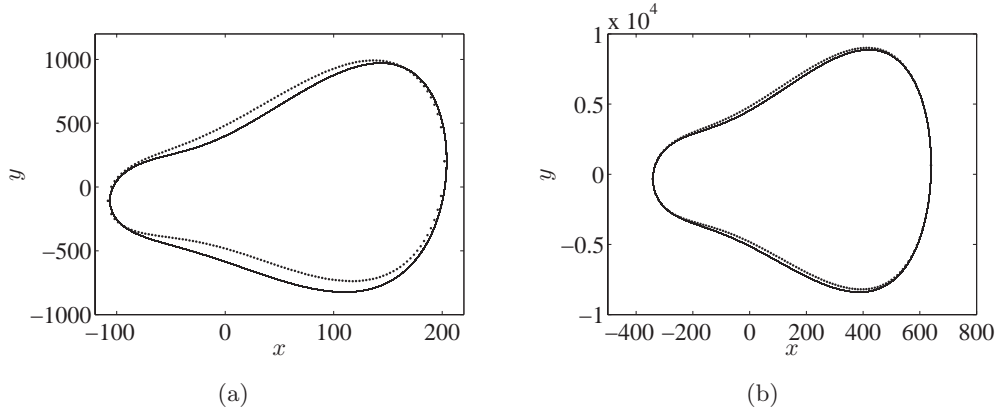
where x_1 and x_2 are two zeros of $-\frac{1}{2}X_0^4 + (1 - Y_0)X_0^2 + 2CX_0 + \frac{1}{2}K_0 = 0$ with $x_1 < x_2$. Using the period T in (27), the constants K_0 and Y_0 for the limit cycle can be computed by imposing the condition that the limit cycle ϕ_1 is also periodic as

$$\begin{aligned} \int_0^T \dot{\phi}_1 dt &= 0: \\ \int_{x_1}^{x_2} \frac{2X_0^2(Y_0 - X_0^2) + 4(\sigma + 1)Z_0^2}{\sqrt{-\frac{1}{2}X_0^4 + (1 - Y_0)X_0^2 + 2CX_0 + \frac{1}{2}K_0}} dX_0 \\ &= 0 \end{aligned} \quad (28)$$

and for Y_1

$$\begin{aligned} \int_0^T \dot{Y}_1 dt &= 0: \\ \int_{x_1}^{x_2} \frac{-Y_0 + X_0^2}{\sqrt{-\frac{1}{2}X_0^4 + (1 - Y_0)X_0^2 + 2CX_0 + \frac{1}{2}K_0}} dX_0 \\ &= 0. \end{aligned} \quad (29)$$

Although the integrals (28) and (29) are analytically solvable since they are kinds of elliptic integrals, the constants Y_0 and K_0 are obtained numerically due to their very cumbersome analytical expressions except for $C = 0$. Figure 6 shows numerically computed constants Y_0 and K_0 as a function of C at $\sigma = 15$. The numerical code to compute the constants Y_0 and K_0 was validated with [Shimizu, 1979] at $C = 0$. Using these constants, we obtain asymptotic limit cycles (23) and we can transform back to original variables x , y and z by

Fig. 7. Limit cycles on the x - y plane (solid line) and asymptotic limit cycles (dots) for $C = 0.0045$ and (a) $(r, c) = (10000, 24643.8)$ and (b) $(r, c) = (100000, 779411.2)$.

the transformation (7) for given values of parameters r and c .

Figure 7 shows examples of limit cycles obtained numerically and asymptotically for different parameters r and c . It is clearly shown that the asymptotic limit cycles converge to the limit cycles as the parameter r becomes large. Therefore, we see that all the solutions converge to periodic limit cycles for sufficiently large values of r and c . This explains why the chaotic regime is enclosed by the regimes of periodic solutions.

5. Conclusions

In this paper, we investigated the set of nonlinear ordinary differential equations of the Ehrhard–Müller system. From the stability analysis, regimes of stability were obtained and the corresponding dynamics of solutions for each regime was derived. In the regime where all the equilibrium points are unstable, we numerically investigated periodic and chaotic behaviors of the equations by computing the periodicity diagram in wide ranges of parameters r and c where the period is defined by the number of local maximum values of variable z . Regimes of both periodic and chaotic solutions are observed and interestingly, the chaotic regime is enclosed by the periodic regimes while it contains periodic regimes with various shapes such as curved bands, shrimp-shape islands, narrow periodic windows, etc. The chaotic regime was also analyzed by the Lyapunov exponents such that the maximum Lyapunov exponent becomes positive in the chaotic regime while it becomes zero in the regime of periodic solutions. Moreover, the enclosure of the chaotic regime by the periodic regimes was explained by an asymptotic analysis which gives an asymptotic expression of periodic limit cycles for large parameters r and c . The results in this paper are similar to those of the Lorenz–Stenflo system [Xavier & Rech, 2010; Park *et al.*, 2015] which do not exhibit chaotic behaviors when the control parameters are sufficiently large. In this way, further investigations should be followed on other nonlinear systems in wide ranges of their control parameters to see if the chaotic solutions disappear for large values of parameters. Moreover, the Ehrhard–Müller system should be investigated either by experiments or by computational fluid dynamics (CFD) simulations in the parameter space studied in this paper to see if the chaotic behavior is still observed as in previous

experiments [Ehrhard & Müller, 1990] or is suppressed for large values of r and c . Various periodic regimes both inside the chaotic regime and along the boundary of the chaotic regime are also not well understood thus should be investigated in future works.

Acknowledgments

The authors are grateful to three anonymous reviewers for their constructive comments and suggestions which improved the original manuscript. This work was funded by the Korea Meteorological Administration Research and Development Program under Grant KMIPA 2015-5100.

References

- Acosta, R., Sen, M. & Ramos, E. [1987] “Single-phase natural circulation in a tilted square loop,” *Wärmeund Stoffübertragung* **21**, 269–275.
- Albuquerque, H. A., Rubinger, R. M. & Rech, P. C. [2008] “Self-similar structures in a 2D parameter space of an inductorless Chua’s circuit,” *Phys. Lett. A* **372**, 4793–4798.
- Basu, D. N., Bhattacharyya, S. & Das, P. K. [2014] “A review of modern advances in analyses and applications of single-phase natural circulation loop in nuclear thermal hydraulics,” *Nucl. Eng. Design.* **280**, 326–348.
- Bonatto, C., Garreau, J. & Gallas, J. A. C. [2005] “Self-similarities in the frequency-amplitude space of a loss-modulated CO₂ laser,” *Phys. Rev. Lett.* **95**, 143905.
- Christiansen, F. & Rugh, H. H. [1997] “Computing Lyapunov spectra with continuous Gram–Schmidt orthonormalization,” *Nonlinearity* **10**, 1063–1072.
- Dullin, H. R., Schmidt, S., Richter, P. H. & Grossmann, S. K. [2007] “Extended phase diagram of the Lorenz model,” *Int. J. Bifurcation and Chaos* **17**, 3013–3033.
- Ehrhard, P. & Müller, U. [1990] “Dynamical behaviour of natural convection in a single-phase loop,” *J. Fluid Mech.* **217**, 487–518.
- Gallas, J. A. C. [1993] “Structure of the parameter space of the Hénon map,” *Phys. Rev. Lett.* **70**, 2714.
- Gollub, J. P. & Swinney, H. L. [1975] “Onset of turbulence in a rotating fluid,” *Phys. Rev. Lett.* **35**, 927–930.
- Gorman, M., Widmann, P. J. & Robbins, K. A. [1984] “Chaotic flow regimes in a convection loop,” *Phys. Rev. Lett.* **52**, 2241–2244.
- Gorman, M., Widmann, P. J. & Robbins, K. A. [1986] “Nonlinear dynamics of a convection loop: A quantitative comparison of experiment with theory,” *Physica D* **19**, 255–267.

- Lorenz, E. N. [1963] “Deterministic non-periodic flow,” *J. Atmos. Sci.* **20**, 130–141.
- Malkus, W. V. R. [1972] “Non-periodic convection at high and low Prandtl numbers,” *Mém. Soc. Royale de Sci. de Liège* **6**, 125–128.
- Meador, C.-E. E. [2011] “Numerical calculation of Lyapunov exponents for three-dimensional systems of ordinary differential equations,” Master’s thesis, Marshall University.
- Park, J., Lee, H., Jeon, Y.-L. & Baik, J.-J. [2015] “Periodicity of the Lorenz–Stenflo equations,” *Phys. Scr.* **90**, 065201.
- Shil’nikov, A. L. & Shil’nikov, L. P. [1991] “On the non-symmetrical Lorenz model,” *Int. J. Bifurcation and Chaos* **1**, 773–776.
- Shimizu, T. [1979] “Analytical form of the simplest limit cycle in the Lorenz model,” *Physica A* **97**, 383–398.
- Welander, P. [1967] “On the oscillatory instability of a differentially heated loop,” *J. Fluid Mech.* **29**, 17–30.
- Widmann, P. J., Gorman, M. & Robbins, K. A. [1989] “Nonlinear dynamics of a convection loop II. Chaos in laminar and turbulent flows,” *Physica D* **36**, 157–166.
- Xavier, J. C. & Rech, P. C. [2010] “Regular and chaotic dynamics of the Lorenz–Stenflo system,” *Int. J. Bifurcation and Chaos* **20**, 145–152.
- Yorke, J. A. & Yorke, E. D. [1981] “Chaotic behaviour and fluid dynamics,” *Hydrodynamic Instabilities and the Transition to Turbulence* (Springer), pp. 77–95.
- Yorke, J. A., Yorke, E. D. & Mallet-Paret, J. [1987] “Lorenz-like chaos in a partial differential equation for a heated fluid loop,” *Physica D* **24**, 279–291.
- Yu, M. Y., Zhou, C. T. & Lai, C. H. [1996] “The bifurcation characteristics of the generalized Lorenz equations,” *Phys. Scr.* **54**, 321–324.
- Zhou, C., Lai, C. H. & Yu, M. Y. [1997a] “Bifurcation behavior of the generalized Lorenz equations at large rotation numbers,” *J. Math. Phys.* **38**, 5225–5239.
- Zhou, C., Lai, C. H. & Yu, M. Y. [1997b] “Chaos, bifurcations and periodic orbits of the Lorenz–Stenflo system,” *Phys. Scr.* **55**, 394–402.
- Zhu, J. & Tian, Y.-P. [2005] “Stabilizing periodic solutions of nonlinear systems and applications in chaos control,” *IEEE Trans. Circ. Syst.-II* **52**, 870–874.
- Zvirin, Y. [1982] “A review of natural circulation loops in pressurized water reactors and other systems,” *Nucl. Eng. Design* **67**, 203–225.